ISBN: 978-3-95450-225-7 ISSN: 2673-5571 doi:10.18429/JACoW-HB2021-MOP04

STATUS OF THE JAEA-ADS SUPERCONDUCTING LINAC DESIGN

B. Yee-Rendon*, Y. Kondo, J. Tamura, S. Meigo and F. Maekawa
JAEA/J-PARC, Tokai-mura, Japan

Abstract

The Japan Atomic Energy Agency (JAEA) is working in the research and development of an Accelerator Driven Subcritical System (ADS) for the transmutation of nuclear waste. To this end, JAEA is designing a 30 MW cw proton linear accelerator (linac) with a beam current of 20 mA. The JAEA-ADS linac starts with a Normal Conducting (NC) up to an energy of 2.5 MeV. Then, five Superconducting (SC) sections accelerate the beam up to 1.5 GeV. The biggest challenge for this ADS linac is the stringent reliability required to avoid thermal stress in the subcritical reactor, which is higher than the achieved in present accelerators. For this purpose, the linac pursues a strong-stable design that ensures the operation with low beam loss and fault-tolerance capabilities to continue operating in case of failure. This work presents the beam dynamics results toward achieving high reliability for the JAEA-ADS linac.

INTRODUCTION

The Japan Atomic Energy Agency (JAEA) is doing R&D in an Accelerator Driven Subcritical System (ADS) for the transmutation of minor actinides to reduce the long lifetime and high radiotoxicity of nuclear waste. The JAEA-ADS project is composed of a 30 MW cw proton linac, a spallation target, and an 800 MW thermal power subcritical reactor [1], as shown in Fig. 1.

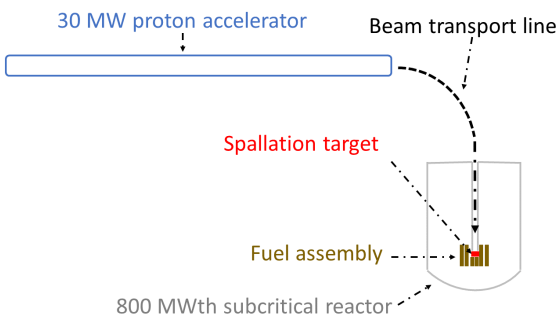

Figure 1: General scheme for the ADS.

A summary of the main specifications of the JAEA-ADS linac is provided in Table 1. Among them, the restricted number of beam trips is the main challenge for the ADS, which is beyond the present high-intensity linacs [2]. Thus, the JAEA-ADS linac seeks a reliability-oriented accelerator by achieving a robust beam optics design and fault-tolerance capabilities [3].

BEAM OPTICS DESIGN

The beam optics design pursues strict control beam loss and beam properties such as energy spread and emittance growth; simple lattice arrangement; operation with de-rated elements to reduce the failure probabilities and applied fault-tolerance schemes.

Table 1: Main Characteristics of the JAEA-ADS Accelerator

Parameter		Beam trip duration
Particle	Proton	
Beam current (mA)	20	
Beam energy (GeV)	1.5	
Duty factor (%)	100 (cw)	
Beam loss (W/m)	< 1	
Length (m)	429	
Beam trips per year [4]	2×10^4	≤ 10 s
	2×10^3	from 10 s to 5 min
	42	> 5 min

Figure 2 shows that JAEA-ADS linac has a normal conducting (NC) part, a so-called Injector, and a superconducting (SC) part known as the Main Linac. The Main Linac employs five groups of SC cavities to achieve high accelerating efficiency and compact design. The Half Wave Resonator (HWR) and Single Spoke Resonator (SSR) use a configuration solenoid-cavity inside the cryomodule. For the HWR region, the period is composed of one solenoid and one cavity; on the contrary, the SSR periods have two SC cavities for SSR1 and three for SSR2. Five-cell Elliptical Resonators (EllipRs) employ doublet NC quadrupoles with three and five SC cavities per cryomodule for EllipR1 and EllipR2, respectively [5].

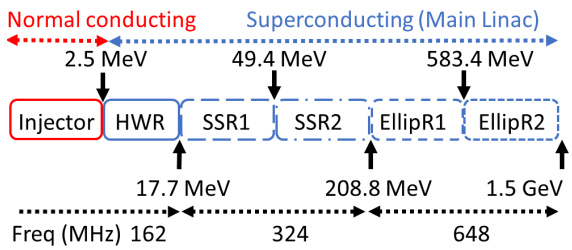

Figure 2: Linac lattice configuration.

At the normal operation, the maximum accelerating gradient (E_{acc}) for the SC cavities was chosen to operate with an electric peak up to 30 MV/m to reduce the possibility of a malfunction in the cavity. Moreover, in case of an SC cavity failure, it enables the increase of E_{acc} to apply for fault-tolerance compensations.

The beam optics was developed using the programs GenLinWin and Tracewin [6]. The beam loss was minimized by reducing the beam halo and emittance growth. This was achieved by pursuing an equipartitioning model, avoiding parameter resonances, among others [5]. The lattice design was optimized first in ideal conditions, i.e., without errors,

* byee@post.j-parc.jp

ISBN: 978-3-95450-225-7 ISSN: 2673-5571 doi:10.18429/JACoW-HB2021-MOP04

Table 2: Parameters of the Main Linac

Parameters	
Input ε_x (π mm mrad)	0.24
Input ε_y (π mm mrad)	0.23
Input ε_z (π MeV deg/mm mrad)	0.08/0.39
Number of Cavities	293
Number of magnets	153
Length (m)	416

tracking large beam distributions with 1×10^7 macroparticles obtained from the RFQ design [7]. Table 2 presents the relevant parameters of the Main Linac. This ideal case is known as the Ideal Machine (IM) case. The IM case did not record beam loss; furthermore, it has reasonable control of the normalized root-mean-square ε, see Fig. 3.

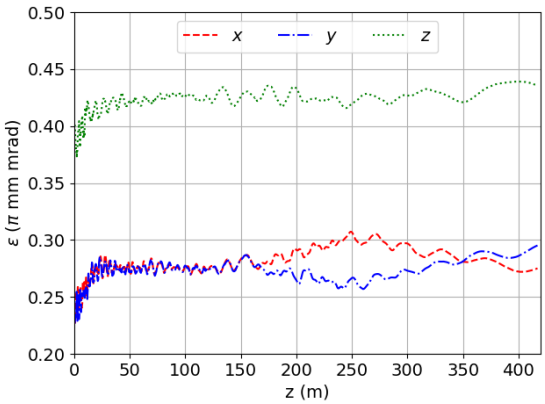

Figure 3: Normalized rms emittance in the linac.

Then, the robustness of the lattice was tested using element errors and input beam errors (IBE). The former are misalignments and parameters fluctuations of the cavities and magnets. They are divided as statics elements errors (SEE) and dynamics element errors (DEE). On the contrary, IBEs are errors from Injector part such as emittance growth and energy fluctuations. Reference [8] provides a detailed explanation of the errors and their application. Figures 4 and 5 present a comparison of the ε growth and the maximum radial envelopes for the error cases and the IM one. From all the error cases simulated, only the static errors registered beam loss; however, the corresponding maximum power loss was 20 mW/m, two orders of magnitude lower than the limit for hand-on maintenance.

FAULT-TOLERANCE

Fault-tolerance is achieved by using parallel or serial redundancy. For the former, the linac lattice is partially or completely duplicated. In contrast, serial redundancy exploits the modularity of the linac by using the neighbors' elements of the faulty element to compensate for the unwanted effect produced by the faulty one. This study was focused on serial redundancy; however, the general strategy is to use both schemes to decrease the duration and the number of beam trips. Figure 6 illustrates the serial redundancy

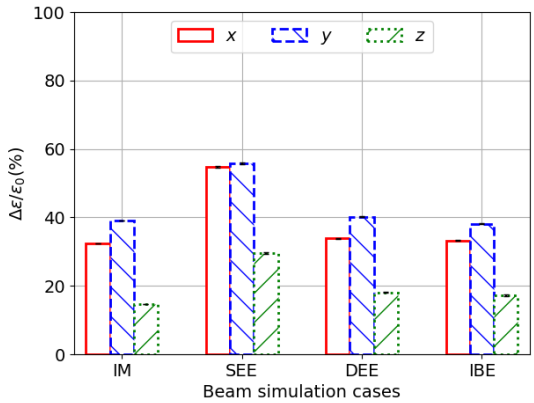

Figure 4: Normalized rms emittance growth for the different beam simulation cases.

for a faulty SC cavity; nevertheless, the compensation for a magnet failure follows the same proceeding.

Based on the Fault-tolerance schemes reported by Biarrotte [9, 10], two schemes were applied: beam stopping compensation scheme and beam continue compensation scheme. Figure 7 provides a summary of both schemes. The main difference between both schemes is that the first one begins with the compensation after the faulty element is detuned. Subsequently, the compensation setting is less complex because it does not require to be updated. On the contrary, the continue case starts the compensation when the faulty element is acting in the beam. Thus, the compensation settings need to be continually updated according to the transient behavior of the faulty element; consequently, the scheme becomes more complex and requires a large RF power budget.

The nonstop beam scheme is more attractive than the stopped one because it implies the beam operation is not interrupted; however, it is more challenging. Nevertheless, when the fault element is detuned, both cases have the same compensation settings. The three main challenges of both schemes are a fast-reliable diagnostic, an accurate large compensation database, and fast control system. In addition, these configurations are temporary; thus, after recovery of the fault, the element settings will be returning to the design configuration at a certain proper time.

The schemes were optimized to fulfill the next requirements:

- Beam loss < 1 W/m.
- Energy difference < $\pm$1%.
- $\Delta\varepsilon_{trans}/\varepsilon_{0,trans} < 2$.
- Mismatch < 0.4.
- Increase of E_{acc} up to 20 % and 50 % for the stopping and continue case, respectively.
- Increase of the magnetic field up to 20 %.

The energy, ε, and mismatch are with respect to the design case, also knows as the IM case. The values were calculated using beam tracking simulations using 2×10^5 macroparticles.

The beam stopping strategy has been reported in previous conferences [11, 12]. Figure 8 presents the compensation

ISBN: 978-3-95450-225-7 ISSN: 2673-5571 doi:10.18429/JACoW-HB2021-MOP04

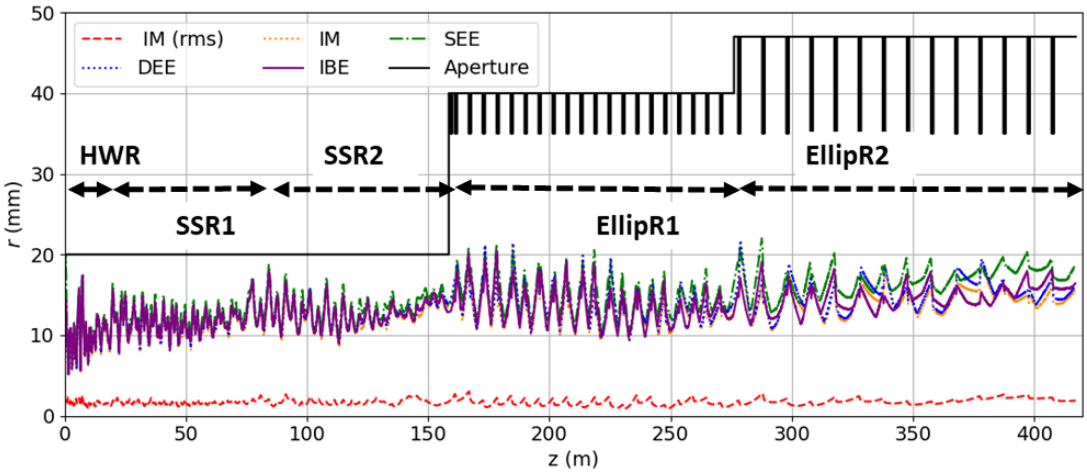

Figure 5: Maximum radial beam size along the Main Linac for the different cases. The aperture and the rms size, for the IM case, are included as a reference.

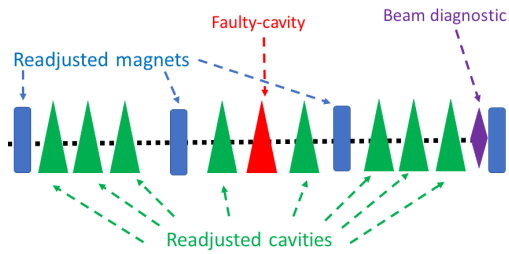

Figure 6: Serial redundancy scheme.

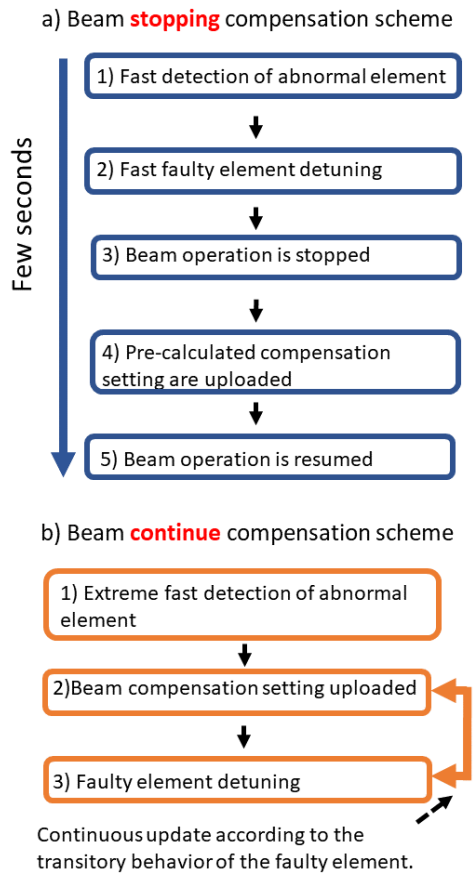

Figure 7: Serial redundancy strategies.

for a failure in the last cavity of the EllipR1 section using this scheme. E_{acc} and ϕ_s around the faulty SC cavity are re-adjusted to restore the beam energy at the closest downstream period. Studies indicated that this procedure is suitable for faulty elements in the last four sections of the Main Linac SC cavity. The overall results registered no beam loss, an energy difference below 0.3 %, and the largest mismatch was 0.17. In addition, Fig. 9 presents the transverse and longitudinal ε growth for the worst compensation performance in a cavity and magnet failure for the SSRs and EllipRs section. This strategy is effective for decreasing the number of beam trips that take longer than 10 s.

For the beam continue compensation scheme, only SC cavities were tested. In addition, the transient behavior of the cavities was computed considering only the detuning contributions of the cold tuning system and Lorentz force [10]. For instance, a failure at the end of the SSR1 section is discussed below. Figure 10 shows the transient behavior of the E_{acc} and ϕ_s for the faulty cavity. The failure was arbitrarily chosen to occur 500 µs after the simulation started, and 1 ms later, the cavity operated with almost the same E_{acc} as the design; but, ϕ_s suffered a change of -150°. Figure 11 presents the output energy dropped to zero after 230 µs after the failure. It suggests that the adjustment scheme could start at 230 µs after the failure, but beam loss is recorded at 160 µs later the failure occurred. After a trade-off among a lower number of cavities, stable compensation, and realistic response time, it was decided to use two SC cavities before and three SC after the faulty SC cavity and begin the adjustment 130 µs after the failure.

Figure 12 shows that the final energy becomes stable after some hundred microseconds after the compensation is applied. Between the failure starts until a stable compensation is reached, the particles are transported through the linac with an acceptable beam performance.

ISBN: 978-3-95450-225-7 ISSN: 2673-5571 doi:10.18429/JACoW-HB2021-MOP04

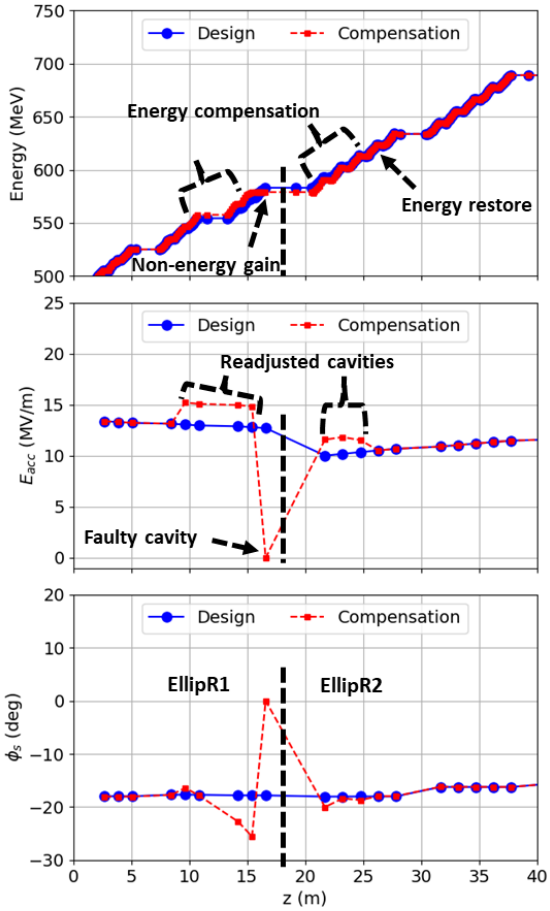

Figure 8: Compensation scheme for the failure in the last EllipR1's cavity. The black-dotted vertical line indicates the transition between EllipR1 and EllipR2 regions.

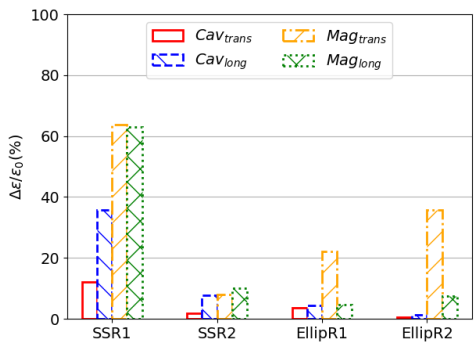

Figure 9: Transverse and longitudinal ε growth for the worst compensation case in SC regions, excluding the HWR section.

Additionally, Fig. 13 presents the maximum radial envelopes for the design, beam failure, and compensated case. In the beam failure scenario, i.e., without compensation, the beam envelope reached the aperture at the SSR2 section. On the contrary, the envelope for the beam compensated has a similar evolution as the design one. The largest radial beam envelopes in Fig. 13 are smaller than Fig. 5 because the number of macroparticles was reduced as a compromise

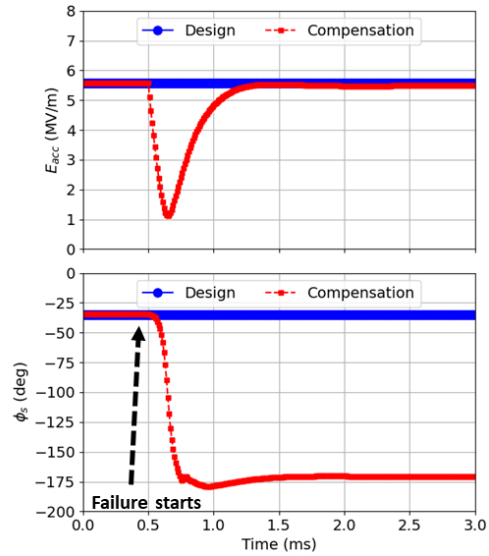

Figure 10: E_{acc} (top) and ϕ_s (bottom) for the faulty cavity.

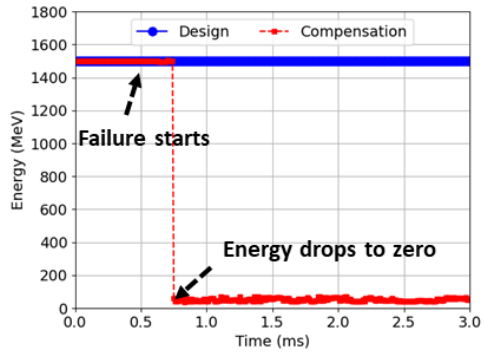

Figure 11: Output energy for the failure case.

between high statistics and the available computational resources. This procedure showed the feasibility of continuing operating the linac in the presence of faulty cavities.

CONCLUSION

The JAEA-ADS linac pursues a robust beam optics design with fault-tolerance capabilities to avoid thermal stress in the subcritical reactor. The multiparticle tracking studies showed a beam operation with beam losses of 20 mW/m in

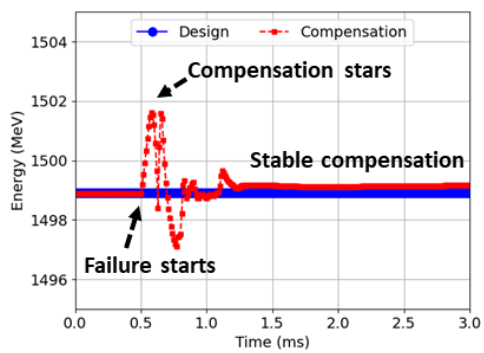

Figure 12: Final energy for the compensation case.

ISBN: 978-3-95450-225-7 ISSN: 2673-5571 doi:10.18429/JACoW-HB2021-MOP04

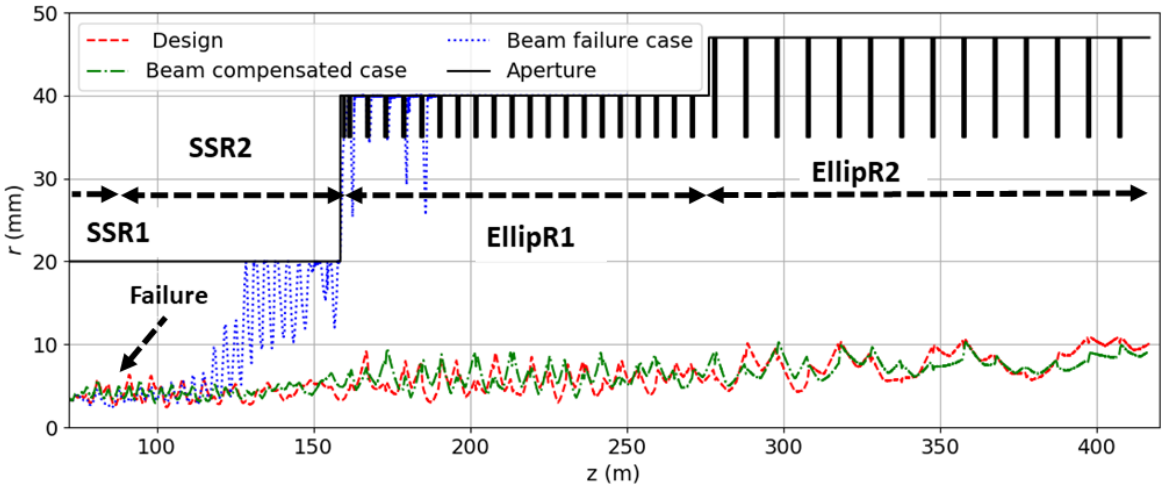

Figure 13: Maximum radial beam size from some periods before the failure starts to the end of the linac.

error cases. In addition, the beam optics design has proper control of the beam envelopes and emittance growth.

The fault-tolerance analysis proved serial redundancy could be applied from the spoke section to the end of the linac to fulfill the stringent reliability with acceptable beam output properties and without compromise the cavity operation or neither a significant increase of the RF power budget. These schemes indicate the possibility of a total or partial reduction of the failure time in the SC cavities and magnets of the linac. Therefore, they represent key conditions to meet the strict reliability of the ADS project.

ACKNOWLEDGMENTS

The authors would like to thank to the members of the JAEA-ADS for their comments and suggestions. This work is supported by the Subvention for ADS development.

REFERENCES

[1] K. Tsujimoto *et al.*, "Neutronics design for lead-bismuth cooled accelerator-driven system for transmutation of minor actinide", *J. Nucl. Sci. Technol.*, vol. 41, no. 21, p. 21, Jan. 2004. doi:10.1080/18811248.2004.9715454

[2] D. Vandeplassche and L. Medeiros-Romao, "Accelerator Driven Systems", in *Proc. 3rd Int. Particle Accelerator Conf. (IPAC'12)*, New Orleans, LA, USA, May 2012, paper MOYAP01, pp. 6–10.

[3] J.L. Biarrotte, "Reliability and fault tolerance in the European ADS project", CERN, Geneva, Switzerland, Rep. CERN-2013-001.481, Jun. 2011.

[4] H. Takei, K. Nishihara, K. Tsujimoto, and H. Oigawa, "Estimation of acceptable beam-trip frequencies of accelerators for accelerator-driven systems and comparison with existing performance data", *J. Nucl. Sci. Techol.*, vol. 49, p. 384, Sep. 2012. doi:10.1088/00223131.2012.669239

[5] B. Yee-Rendon *et al.*, "Present Status of the R&D of the Superconducting Linac for the JAEA-ADS", *J. Phys. Soc. Jpn.*, vol. 33, p. 011043, March 2021. doi:10.7566/JPSCP.33.011043

[6] GenLinWin Manual, http://irfu.cea.fr/dacm/logiciels TraceWin Manual, http://irfu.cea.fr/dacm/logiciels

[7] Y. Kondo, J. Tamura, and B. Yee-Rendon, "Reference Design of the RFQ for JAEA ADS Linac", *JPS Conf. Proc.*, vol. 33, p. 011015, March 2021. doi:10.7566/JPSCP.33.011015

[8] B. Yee-Rendon, J. Tamura, Y. Kondo, F. Maekawa, S. Meigo, and H. Oguri, "Error Studies for the JAEA-ADS Linac" , in *Proc. 17th Annual Meeting of Particle Accelerator Society of Japan (PASJ'20)*, Matsuyama, Japan, Sept. 2020, paper WEOT01, pp. 33–37.

[9] J.-L. Biarrotte, M. Novati, P. Pierini, H. Safa, and D. Uriot, "Beam Dynamics Studies for the Fault Tolerance Assessment of the PDS-XADS Linac Design", in *Proc. 9th European Particle Accelerator Conf. (EPAC'04)*, Lucerne, Switzerland, Jul. 2004, paper TUPLT057, pp. 1282–1284.

[10] J.-L. Biarrotte and D. Uriot, "Dynamic compensation of an rf cavity failure in a superconducting linac", *Phys. Rev. ST. Accel. Beams*, vol. 11, p. 072803, July 2008. doi:10.1103/PhysRevSTAB.11.072803

[11] B. Yee-Rendon *et al.*, "Progress on SRF Linac Development for the Accelerator-Driven Subcritical System at JAEA", in *Proc. 20th International Conf. on RF Superconductivity (SRF'21)*, USA., July 2021, paper TUPFAV001, to be published.

[12] B. Yee-Rendon *et al.*, "Fast Fault Recovery Scenarios for the JAEA-ADS Linac", in *Proc. 18 th Annual Meeting of Particle Accelerator Society of Japan (PASJ'21)*, Japan, Aug. 2021, paper TUOA01, to be published.